MOLECULAR PHYSICS REPORTS **40** (2004) 72-78

RECENT DEVELOPMENTS AND FUTURE OF SOFT MAGNETS WITH NANOCRYSTALLINE $Cr_{23}C_6$-TYPE PHASE

B. IDZIKOWSKI, A. SZAJEK, AND S. KOSTYRYA

Institute of Molecular Physics, Polish Academy of Sciences
M. Smoluchowskiego 17, 60-179 Poznań, Poland

Abstract: A comprehensive review of our recent experimental and theoretical developments in the processing of nanocrystalline soft magnetic materials made from amorphous precursor with nominal chemical composition of $Fe_{81-x-y}Ni_xZr_7B_{12}Au_y$ (x = 10-40, 64; y = 0, 1) is given. The transformation from the amorphous into the nanocrystalline state was investigated by the transmission Mössbauer spectroscopy (MS) and magnetic measurements (VSM). Due to annealing in amorphous matrix appears fine grain fraction of magnetically ordered metastable cubic $Fe_x(Ni\ Co)_{23-x}B_6$ phase. The relationship between the structures of the metastable and equilibrium phases and their transformations are discussed. Magnetic behaviour of the ordered phases was studied by *ab-initio* calculations. Anomalously high magnetic moments of Fe atoms were found in some inequivalent positions in the crystal structure.

1. INTRODUCTION

This paper summarizes our the most recent experimental and theoretical developments in the processing of soft magnets with $Cr_{23}B_6$-type nanocrystalline phase prepared by annealing in inert atmosphere of amorphous precursors in the form of ribbons. It gives an overview of the relevant classes of extremely soft magnets, *e.g.* FINEMET, NANOPERM and HITPERM, together with a description of the appropriate manufacturing methods and focuses on important parameters for application and its relations to soft magnets with $Cr_{23}B_6$-type phase. Particular attention to the magnetic behaviour of melt-spun samples and then subsequently annealed at different temperatures for one hour to form nanostructure, in comparison with theoretical predictions will be given.

High saturation magnetization can be achieved in many crystalline magnetic materials by increasing of iron concentration. Soft magnetic properties of Fe-based magnets are usually bad because of large magnetocrystalline anisotropy of *bcc*-Fe. Large anisotropy constant of Fe could be suppressed in composite materials by reducing the grain size to the scales of few nanometer. Due to the magnetic exchange interactions nanocrystalline alloys consisting of soft magnetic grains placed in amorphous matrix can reveal a smooth magnetization curve with extremely small values of coercive force. A novel approach employed in the development of soft magnetic materials is to reduce ratio of the structural correlation length depending on the grains' sizes to the ferromagnetic correlation length in range of domain wall width.

Up to now nanocrystalline alloys, produced by partial crystallization of amorphous precursors, exhibit a multiphase structure with nanocrystalline body-centred-cubic (*bcc*) grains dispersed into the residual amorphous matrix. Well-known soft magnetic nanocrystalline alloys consist of the homogeneous phase of nanosized *bcc*-Fe(Si), *bcc*-Fe, or *bcc*-(FeCo) grains (see *e.g.* [1-3]) with 3-15 nm in diameter. During the devitrification processes amorphous part of

alloys becomes inhomogeneous showing some, sometimes significant, gradients of chemical composition. However, due to magnetic exchange interactions *via* this matrix, nanocrystalline systems consisting of magnetic grains can show low coercivities. This magnetic softening phenomenon in nanocrystalline materials was explained by Herzer [4], who proposed the successful extension of previous random anisotropy models [5, 6].

2. EXPERIMENTAL

Melt-spun alloys with the appropriate nominal composition $Fe_{81-x-y}Ni_xZr_7B_{12}Au_y$ (x = 10-40, 64; y = 0, 1) were prepared by a single roller technique in Ar protective atmosphere. High-purity elements were used to make starting pre-alloys. Each ingot was several times turned over and melted by induction heating in water cooled boat to assure homogeneity. The ribbon was 2-3 mm wide and 35-40 μm thick. The structure of the samples was characterized by XRD analysis in a Seifert diffractometer using Cu-K_α radiation. The crystallization behaviour of as-quenched ribbons was examined by differential scanning calorimetry (DSC) using Netzsch DSC 404 apparatus under flowing Ar at various heating rates for scans up to selected temperatures.

3. RESULTS AND DISSCUSION

A set of similar experimental procedures were applied for investigations and the results were analysed for understanding of nanocrystallization processes in low and high nickel content ribbons containing 7 at.% of Zr and 12 at.% of B. For optimal annealed samples, that means exhibiting the greatest magnetic softness, structural and magnetic properties are compared and discussed.

Crystallization of amorphous $Fe_{81-x}Ni_xZr_7B_{12}$ (x = 10-40) alloys, as investigated by DSC linear-heating curves (not shown here), clearly shows two crystallization stages with two characteristic crystallization temperatures. Such a behaviour is typical for amorphous alloys serving as the precursors for the formation of the nanocrystalline alloys. The crystallization temperatures of the first and second stage depend on alloy composition. They decrease from about 510°C and 730°C for low Ni-content (x = 10) to about 480°C and 650°C for high Ni-content (x=40).

The transmission Mössbauer spectra recorded for the $Fe_{41}Ni_{40}Zr_7B_{12}$ alloy annealed at indicated temperatures for one hour are shown in Fig. 1. As can be seen, the crystalline *bcc*-Fe phase forms in the sample annealed at 470°C, in addition to the amorphous phase (Fig. 1b). Increase of the annealing temperature causes the increase of the spectral contribution of the *bcc*-Fe phase and then at $T_a \geq 570$°C a decrease of this component, associated with the simultaneous change of the spectral component related to the broadened sextet which now corresponds both to the residual amorphous phase and to the Ni-containing nanostructure. The H_{hf} of this sextet slightly decreases which suggests a substantial Ni-content in the nanocrystalline phase (Fig. 1c, 1d). The XRD measurements suggest that the nanograins of the $(FeNi)_{23}B_6$ phase are formed at $T_a \approx 570$°C. At $T_a \approx 595$°C the single line component appears in

the spectrum (Fig. 1e) and the H_{hf} of the magnetic component further decreases. The single-line component dominates in the spectra recorded for T_a = 620-640°C (Fig. 1f). The increase of T_a above the temperature of the second crystallization peak in DSC curve causes complete crystallization of the sample and the single-line component disappears (Fig. 1g, 1h). The phase formed at $T_a \geq$ 700°C (Fig. 1h) is most probably *fcc*-FeNi. The origin of the single-line component (Fig. 1e, 1f) could be related to the superparamagnetic relaxation in the nanograins of FeNi-containing phase as revealed by the gradual transformation of this component to the magnetic pattern at low temperatures. The crystallization behaviour of samples with lower Ni-content (not shown here) proceeds in a simpler way, typical for other NANOPERM-like alloys.

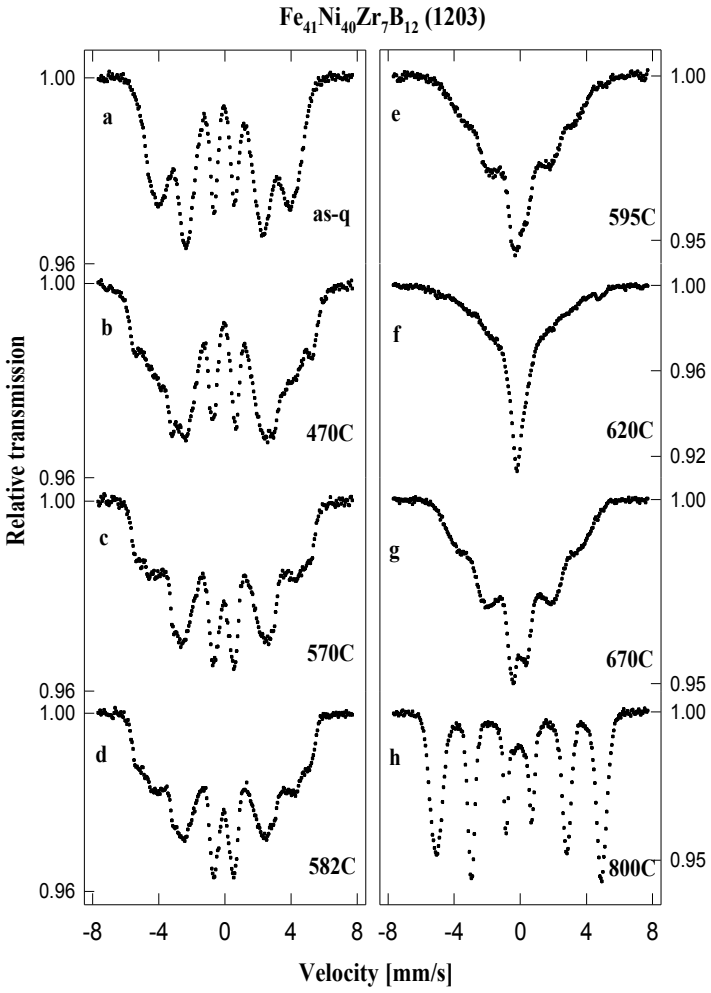

Fig. 1. Room temperature Mössbauer spectra of $Fe_{41}Ni_{40}Zr_7B_{12}$ alloy annealed for one hour at indicated temperatures [7]

For an as-quenched fully amorphous $Ni_{64}Fe_{16}Zr_7B_{12}Au_1$ ribbon DSC isochronal curve with heating rate 20 K/min (not shown here) exhibits also two main exothermic peaks with big similarity to ribbons with lower Ni content [7]. The first crystallization peak onset occurs at $T_1 = 448$°C while the second one is at $T_2 = 492$°C. Up to 900°C on DSC trace no other distinct thermodynamic events were found. Small anomalies around 350°C and 620°C could be connected with magnetic transitions and final crystallization step, respectively. These onset temperatures for primary crystallization are associated with a nucleation process and growth of new crystalline phase(s).

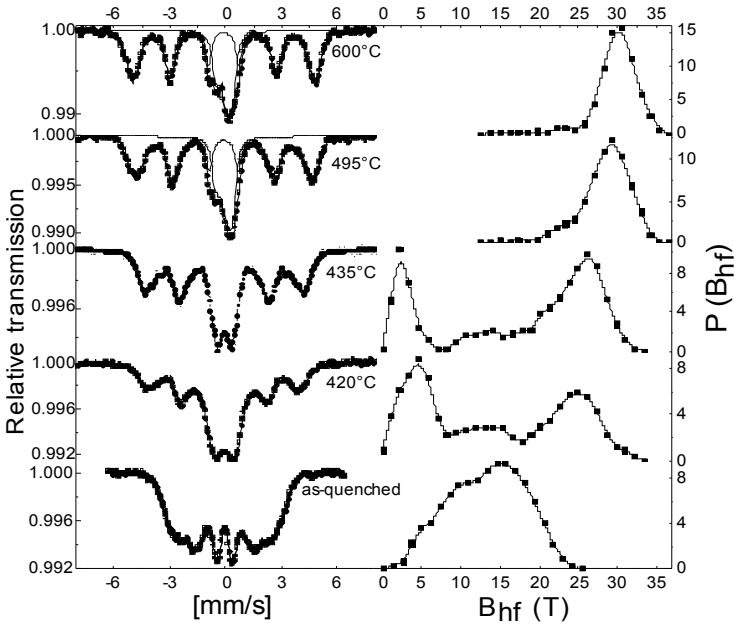

Fig. 2. Mössbauer spectra recorded at 300 K for as-quenched amorphous $Ni_{64}Fe_{16}Zr_7B_{12}Au_1$ alloy and for different nanocrystalline states resulting from heat treatments at indicated temperatures and corresponding hyperfine field distribution [9]

The fitting model consists of a discrete distribution of hyperfine fields which are presented in Fig. 2. In the case of as-quenched amorphous sample, the hyperfine field distribution is shifted towards low fields by comparing to those usually observed on NANOPERM-like amorphous alloys: such a reduction is unambiguously attributed to the presence of Ni atoms homogeneously distributed in the amorphous matrix. The mean hyperfine field, estimated at about 14 T, is qualitatively explained by the large Ni content. For the nanocrystalline states, the hyperfine structure could be interpreted in conjunction with the X-ray diffraction results. XRD investigations confirm increasing presence of $Cr_{23}C_6$-like phases after annealing at temperatures close above second crystallization peak which is visible on DSC curve.

The shift of the high field peak towards high fields is attributed to the progressive transformation of the amorphous matrix into crystalline *fcc*-FeNi grains and then into crystalline $(FeNi)_{23}B_6$ grains. Indeed, the addition of Ni into a Fe matrix favours the presence of different iron neighbours giving rise to broadened sextet lines and a decrease of the mean magnetic moment at Fe site, *i.e.* of the hyperfine field. In addition, recent calculations in $Fe_{23}B_6$, $Ni_{23}B_6$ and $(FeNi)_{23}B_6$ allow the magnetic moment at the two main Fe sites to be estimated. Assuming that 2.2 μ_B corresponds to a hyperfine field of 33 T, one expects two hyperfine fields at 33 T and 27.8 T, which is successfully achieved when considering a set of four magnetic components, the two other ones being attributed to the atomic disorder around ^{57}Fe site. In addition, the Ni enrichment of the amorphous matrix is fairly consistent with the presence of a low field component which progressively transforms into a paramagnetic phase. Thus, the Mössbauer data agree with XRD data. One can derive from present study the evolution of the volumetric crystalline fraction in terms of Fe content.

Figure 3 shows the temperature dependence of magnetization for $Ni_{64}Fe_{16}Zr_7B_{12}Au_1$ alloy taken in external magnetic field of 300 mT. Curie temperature of as-quenched ribbon is 405 K and slightly decreases for the amorphous fraction of partially recrystallized at 420°C and 435° C samples while low temperature magnetization is nearly the same. Heat treatment at the temperature range from 460°C to 500°C causes formation of the nanostructure with optimal soft magnetic properties (H_c of about several Oe and relative high saturation magnetization at room temperature), good thermal stability of the structure.

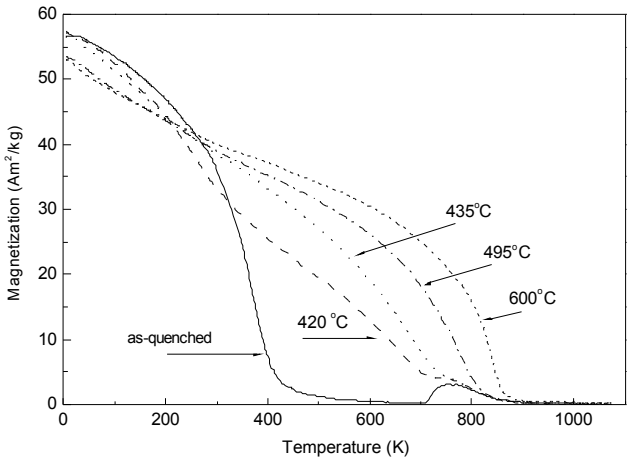

Fig. 3. Magnetization *versus* temperature for melt-spun $Ni_{64}Fe_{16}Zr_7B_{12}Au_1$ alloy in as-quenched state and after annealing at indicated temperatures [9]

For comparison of magnetic measurements with theory the spin polarized tight binding linear muffin-tin orbital method in the atomic sphere approximation [10, 11] was used to compute the electronic band structure of $Fe_{23-x}(Co\ Ni)_xB_6$ (x = 0, 1) compounds. Details of computations are available in Ref. [8]. The shape of the total and local densities of states (DOS) depends on the type of atom, its localization and local environment. The values of total DOS at the Fermi level E_F are equal to 10.59 and 17.50 states/(eV f.u.) for $Fe_{23}B_6$ and $Ni_{23}B_6$ compounds, respectively (see Figs. 4 and 7 in [8]). Because of large number of *d* electrons,

they provide the main contribution to the total DOS for $E = E_F$ (about 90%). The calculated total magnetic moments for $Fe_{23}B_6$ and $Ni_{23}B_6$ compounds are equal to 48.76 and below 10^4 μ_B/f.u., respectively. Local contributions provided by particular atoms are collected in Table 1. For doped systems Fe_{22}(Ni Co)B_6, all possible configurations were considered for location of the impurities, and total energies were compared to find the most stable state. The Ni impurities prefer the 4a site, whereas the Co ones the 48h site.

Table 1. Local magnetic moments for Fe, Ni, Co and B atoms in $Fe_{23-x}T_xB_6$ (T = Ni, Co; x = 0 or 1) compounds (in the parenthesis occupancy). The magnetic moments in $Ni_{23}B_6$ are less than 4×10^5 μ_B/atom [8]

Compound	Magnetic moment [μ_B/atom] for given position				
	4a	8c	48h	32f	24e
$Fe_{23}B_6$ [8]	Fe: 2.98	Fe: 2.55	Fe: 2.22	Fe: 1.88	B: 0.17
$Fe_{22}NiB_6$ [8]	Ni: 0.72	Fe: 2.51	Fe: 2.20	Fe: 1.83	B: 0.17
$Fe_{22}CoB_6$	Fe1(1):3.00	Fe2(1):2.56	Fe3(1/6) :2.22	Fe7(1/2):1.90	B1(1/3):0.16
			Fe4(1/12):2.33	Fe8(1/4):1.89	B2(1/3):0.17
			Fe5(1/3): 2.26	Fe9(1/4):1.89	B2(1/3):0.17
			Fe6(1/3): 2.23		
			Co(1/12): 1.47		

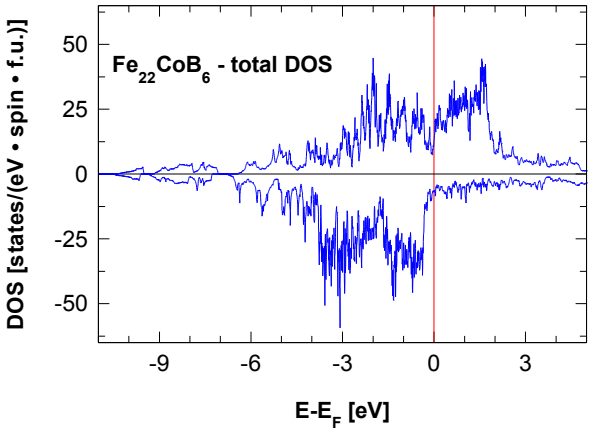

Fig. 4. Total spin projected DOS plots for $Fe_{22}CoB_6$ compound

Location of the Co impurity in the 48h site breaks the starting symmetry and additional inequivalent atoms appear within the sites 48h, 32f, and 24e. Especially high values of magnetic moments are located on Fe(4a) and Fe(8c) atoms, higher than for bulk *bcc*-Fe system (about 2.2 μ_B/atom). The values of magnetic moments depend on local environment of Fe atoms: types of neighbours and interatomic distances. In the case of the 4a and 8c positions, larger than for *bcc*-iron interatomic distances lead to larger Wigner-Seitz (WS) radii and larger magnetic moments. These data can be interpreted qualitatively as showing a tendency toward

localization of the *d* electrons [12]. With increasing WS radii, the magnetic moments approach values closer to the value the moment of an isolated Fe atom. Similar situation for Ni(4a) atom in $Fe_{22}NiB_6$ compound. Its magnetic moment is equal to 0.72 μ_B/atom (in *fcc*-Ni about 0.6 μB/atom). Increasing number of neighbouring boron atoms reduces magnetic moment of iron. In the case of $Ni_{23}B_6$ compound the magnetic moments are reduced practically to zero. The values of total DOS at the Fermi level E_F for doped system are equal to 25.18 and 19.49 states/(eV f.u.) for Ni and Co, respectively (for Ni impurity see Fig. 5 in [8] and Fig. 4 in this paper for Co impurity).

4. CONCLUSIONS

We have studied the influence of annealing temperature on nanostructure formation and magnetic behaviour of amorphous and nanocrystalline Ni-containing alloys. The initial temperatures of crystallization were determined by DSC and VSM measurements. After annealing, ribbons became magnetically soft.

Room temperature ^{57}Fe Mössbauer results show distribution of hyperfine fields consistent with FeNi atomic disorder in the crystalline phase and with magnetization data. Saturation magnetization doesn't depend very much on crystal structure (even in amorphous or nanocrystalline states).

Band structure calculations showed that the local magnetic moments of Fe, Ni, and Co atoms in $Fe_{23-x}T_xB_6$ (T = Ni, Co; $x = 0$ or 1) compounds depend on their local environments. The Ni and Co additions in $Fe_{22}TB_6$ (T = Ni, Co) prefer 4a and 48h sites, respectively. The iron magnetic moments are enhanced in 4a and 8c positions. Similar situation is for Ni(4a) atoms. The nickel moments in $Ni_{23}B_6$ compound are reduced, even to zero. Presence of this metastable phase as nanocrystalline fraction in amorphous matrix is responsible for soft magnetic behaviour of these composites.

References

[1] Y. Yoshizawa, S. Oguma, and K. Yamauchi, J. Appl. Phys. **64**, 6044 (1988).
[2] K. Suzuki, A. Makino, A. Inoue, T. Masumoto, J. Appl. Phys. **70**, 6232 (1991).
[3] M. A. Willard, D. E. Laughlin, M. E. McHenry, D. Thoma, K. Sickafus, J. O. Cross, and V.G. Harris, J. Appl. Phys. **84**, 6773 (1998).
[4] G. Herzer, Phys. Scr. **T49**, 307 (1993).
[5] R. Alben, J. J. Becker, and M. C. Chi, J. Appl. Phys **49**, 1653 (1978).
[6] R. Harris, M. Plischke and M. J. Zuckermann, Phys. Rev. Lett. **31**, 160 (1973).
[7] M. Kopcewicz, B. Idzikowski, and J. Kalinowska, J. Appl. Phys. **94**, 638 (2003).
[8] B. Idzikowski and A. Szajek, Mater. Sci.-Poland **21**, 73 (2003).
[9] B. Idzikowski, A. Szajek, J.-M. Greneche, and J. Kovač; Appl. Phys. Lett. **85**, 1392 (2004).
[10] O. K. Andersen, O. Jepsen, and M. Šob, *Electronic Structure and its Applications*, edited by M. Yussouff, Springer, Berlin (1987), p. 2.
[11] G. Krier, O. Jepsen, A. Burkhardt, and O. K. Andersen, *The TB-LMTO-ASA Program* (source code, version 4.7).
[12] D. Bagayoko and J. Callaway, Phys. Rev. B **28**, 5419 (1983).